Chinese Chemical Letters 37 (2026) 111357

Contents lists available at ScienceDirect

Chinese Chemical Letters

journal homepage: www.elsevier.com/locate/cclet

# Plasmonic metallic Bi-modified defective $Bi_4Ti_3O_{12}$ nanosheets with upward migrating electrons for efficient photocatalytic NO removal and $NO_2$ inhibition

Wenjie He[a,b], Lin Jing[a], Wendong Zhang[c], Xing'an Dong[b,d], Yan Zou[b], Xin Liu[a], Xin Lv[a], Peng Chen[c], Jiazhen Liao[a,*], Xiao Zhang[c], Rong Xiao[c], Yuechang Wei[e,*]

[a] Chongqing Polytechnic University of Electronic Technology, Chongqing 401331, China
[b] Engineering Research Center for Waste Oil Recovery Technology and Equipment, Ministry of Education, Chongqing Technology and Business University, Chongqing 400067, China
[c] Chongqing Key Laboratory of Green Synthesis and Application, College of Chemistry, Chongqing Normal University, Chongqing 401331, China
[d] College of Physics and Electronic Engineering, Chongqing Normal University, Chongqing 401331, China
[e] State Key Laboratory of Heavy Oil Processing, Key Laboratory of Optical Detection Technology for Oil and Gas, China University of Petroleum, Beijing 102249, China

ARTICLE INFO

*Article history:*
Received 24 December 2024
Revised 22 March 2025
Accepted 20 May 2025
Available online 21 May 2025

*Keywords:*
Plasmonic metallic bismuth
Oxygen vacancy
$Bi_4Ti_3O_{12}$
$NO_2$ inhibition
Photocatalysis mechanism

ABSTRACT

The limited redox capability of photocatalysts often leads to harmful $NO_2$ byproduct formation during photocatalytic NO oxidation. Herein, $Bi_4Ti_3O_{12}$ nanosheets modified with plasmonic metallic bismuth and abundant oxygen vacancies were synthesized *via* an *in-situ* reduction method. The optimized catalyst (BTOR2, with a molar ratio of 40% $NaBH_4$ to $Bi_4Ti_3O_{12}$) achieved a maximum NO removal efficiency of 62.3%, significantly higher than pristine $Bi_4Ti_3O_{12}$ (40.5%) while minimizing $NO_2$ production. The results reveal that the synergistic effects of Bi's plasmonic resonance and oxygen vacancies enhanced visible light absorption and charge separation. The density functional theory (DFT) analysis showed electrons can transfer from $Bi_4Ti_3O_{12}$ to Bi, promoting $O_2$ activation to $^{\cdot}O_2^-$ radicals. *In-situ* diffuse reflectance infrared Fourier transform spectroscopy (DRIFTS) confirmed that light-induced $H_2O$ adsorption was strengthened, improving $^{\cdot}OH$ radical generation. These radicals promoted the selective conversion of activated $NO^-$ to $NO_3^-$, rather than $NO_2$. This work provides valuable insights for advancing research into efficient photocatalysts for air pollution control.

© 2025 Published by Elsevier B.V. on behalf of Chinese Chemical Society and Institute of Materia Medica, Chinese Academy of Medical Sciences.

Over the past half-century, photocatalysis has been widely applied to environmental control [1–3], including antibiotic degradation [4], VOCs removal [5], and Cr(VI)-containing wastewater purification [6]. The performance of photocatalytic reactions depends on factors such as light absorption, electron-hole separation, active radical generation, and surface oxidation capacity. To enhance photocatalytic performance, the photoelectric properties of materials must be adjusted, typically by introducing heteroatoms or composites to disrupt the material's charge balance, thereby improving light absorption, charge separation, and carrier migration [7–10].

The efficient generation of surface-active radicals is essential for pollutant degradation, which requires rapid light response and carrier transfer to the catalyst surface. Researchers have optimized material properties through ion doping, metal loading, and defect construction to improve performance [11–14]. For low-concentration atmospheric NO purification, low-energy consumption photocatalysis is an ideal choice [15]. However, in continuous flow reactors, the catalyst's deep oxidation capacity is limited, and surface deactivation caused by by-products affects NO degradation efficiency [16,17]. Additionally, the by-product $NO_2$, is more toxic than NO, so its suppression in photocatalysis process is crucial for effective NO purification. $Bi_4Ti_3O_{12}$ is an Aurivillius-type layered compound with a high oxidation potential due to the hybridization of Bi 6s and O 2p orbitals, making it a suitable catalyst for NO degradation [18–22]. Modification of $Bi_4Ti_3O_{12}$ with plasmonic metallic bismuth, can improve light absorption and electron mobility [23–25]. Meanwhile, defect sites are often constructed on the surface/interface of materials to decrease the band gap [26–29], and oxygen vacancies (OVs) are the most common defect sites usually constructed for oxide semiconductor modification, which can

* Corresponding authors.
*E-mail addresses:* 202122001@cqcet.edu.cn (J. Liao), weiyc@cup.edu.cn (Y. Wei).

https://doi.org/10.1016/j.cclet.2025.111357
1001-8417/© 2025 Published by Elsevier B.V. on behalf of Chinese Chemical Society and Institute of Materia Medica, Chinese Academy of Medical Sciences.

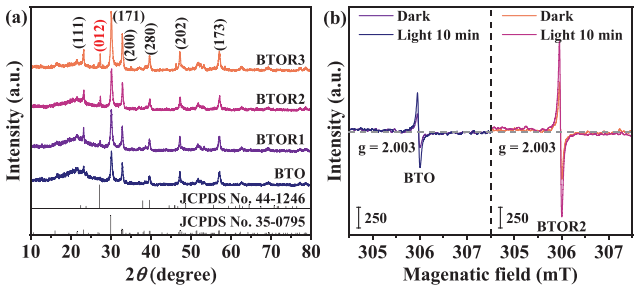



**Fig. 1.** (a) The XRD pattern of BTO and BTORX (X = 1, 2, 3). (b) The low-temperature solid-state EPR spectra of BTO and BTOR2.

play the electrons enrichment center for boosting the generation of active radicals [30–33].

In this work, we developed $Bi_4Ti_3O_{12}$ nanosheets modified with plasmonic metallic bismuth and oxygen vacancies by *in-situ* reduction. This modification significantly enhanced the photoelectric properties of the material. The optimized catalyst, BTOR2, demonstrated superior performance in removing ppb-level NO and suppressing $NO_2$ generation compared to unmodified $Bi_4Ti_3O_{12}$. Mechanisms for active radical generation and deep oxidation were elucidated through electron spin resonance (ESR) and *in-situ* DRIFTS analyses. This study offers insights into enhancing radical generation and pollutant purification *via* photocatalysis.

Phase analysis is shown in Fig. 1a, the X-ray diffraction (XRD) patterns of $Bi_4Ti_3O_{12}$ (BTO) and Bi-modified defective $Bi_4Ti_3O_{12}$ nanosheets (BTORX, X = 1, 2, 3 refer to $NaBH_4/Bi_4Ti_3O_{12}$ molar ratios of 20 %, 40 %, and 60 %, respectively) display typical diffraction peaks at $2\theta = 23.3°$, 30.1°, 32.8°, 39.7°, 47.3°, and 57.2°, corresponding to orthorhombic $Bi_4Ti_3O_{12}$ (JCPDS No. 35-0795). After reduction treatment, a new peak at $2\theta = 37.2°$, attributed to hexagonal metallic Bi (JCPDS No. 44-1246), appears in BTOR1, BTOR2, and BTOR3, confirming the successful introduction of metallic Bi. The electron paramagnetic resonance (EPR) analysis was used to quantify oxygen vacancies (OVs) in BTO and BTOR2. Under dark conditions, a Lorentzian line with $g = 2.003$ was observed (Fig. 1b), indicating OVs exist in as-synthesized catalysts [34]. BTOR2 exhibited a stronger magnetic signal than BTO, reflecting higher OVs density due to $NaBH_4$ reduction. OVs can create defect levels, promoting electron transfer between valence and conduction bands, aiding radical species generation [35]. Under 10-min light irradiation, BTOR2 showed a stronger increase in magnetic signal than BTO, indicating higher carrier mobility of BTOR2 under light. All materials exhibited thin sheet-like morphologies (~50 nm thickness, Fig. S1 in Supporting information) with intact structures after reduction (Figs. 2a-e, and h). At 10 nm resolution, BTOR2 showed a heterostructure with metallic Bi clusters (~5 nm, marked in yellow) distributed on $Bi_4Ti_3O_{12}$ nanosheets (Fig. 2i), while BTO displayed a uniform structure (Fig. 2f). Lattice fringes with spacings of 2.7248 Å and 0.9277 Å correspond to the (200) facet of orthorhombic $Bi_4Ti_3O_{12}$ and the (2110) facet of hexagonal Bi, respectively (Figs. 2g and j). These results confirm the successful synthesis of metallic Bi-modified defective $Bi_4Ti_3O_{12}$ nanosheets.

X-ray photoelectron spectroscopy (XPS) analysis was conducted to study the surface composition of BTO and BTORX (X = 1, 2, 3). The XPS survey spectra (Fig. S2a in Supporting information) show Bi, Ti, O, and C elements, confirming the purity of materials. High-resolution spectra for Bi, Ti, and O are shown in Figs. S2b-d (Supporting information). Peaks at 164.4 eV and 159.1 eV correspond to $Bi^{3+}$ (Bi $4f_{5/2}$, $4f_{7/2}$). Metallic Bi peaks were undetected, possibly due to surface oxidation in air. Peaks at 466.2 eV, 464.0 eV, and 458.1 eV correspond to Bi $4d_{3/2}$ ($Bi^{3+}$) [36], Ti $2p_{1/2}$ ($Ti^{4+}$), and Ti $2p_{3/2}$ ($Ti^{4+}$), respectively. The O 1s spectrum shows lattice oxygen

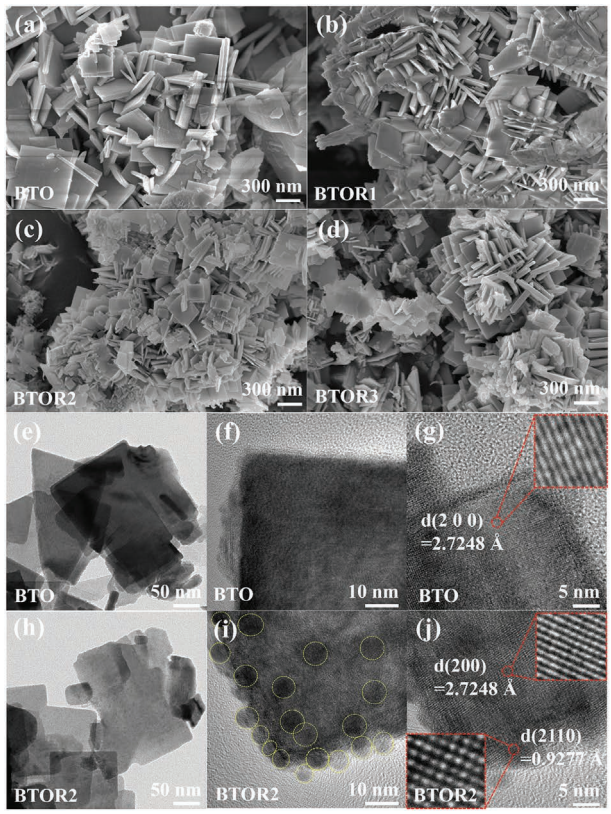



**Fig. 2.** The scanning electron microscope (SEM) images of BTO (a), BTOR1 (b), BTOR2 (c) and BTOR3 (d). Transmission electron microscope (TEM) and high-resolution transmission electron microscope (HRTEM) images of BTO (e-g) and BTOR2 (h-j).

peaks (530.3 eV, 529.8 eV) assigned to Ti-O and Bi-O bonds, and a 532.8 eV peak for adsorbed oxygen (O-H or $H_2O$). These results confirm the chemical composition of the materials.

The photocatalytic NO purification performance of BTO and BTORX (X = 1, 2, 3) was evaluated by the removal of ppb-level NO and the increment of $NO_2$ under light irradiation in a continuous flow reactor. $C_{NO}/C_0$ represents the variation of NO concentration. As shown in Fig. 3a, all materials responded to light and decreased the concentration of the NO within 5 min. The NO removal rates after 30 min for BTO, BTOR1, BTOR2, and BTOR3 were 40.5 %, 46.5 %, 62.3 %, and 53.1 %, respectively. The modified $Bi_4Ti_3O_{12}$ materials outperformed the original $Bi_4Ti_3O_{12}$, and BTOR2 achieving the highest NO removal efficiency of 62.3 % (For comparison, see Table S1 in Supporting information). The $NO_2$ increments after 5 min of illumination were 195, 20, 10, and 405 ppb for BTO, BTOR1, BTOR2, and BTOR3, respectively (Fig. 3b). The release of toxic $NO_2$ by BTO and BTOR3 poses health risks, limiting their practical application. The formation of $NO_2$ is effectively inhibited and NO purification is improved for BTOR2, it indicates that the surface oxidation properties of $Bi_4Ti_3O_{12}$ are optimized by metallic Bi and oxygen vacancies. Stability tests showed that BTOR2 has application potential, and its performance remained stable after five cycles (Fig. S3 in Supporting information).

The efficiency of light absorption and electron-hole pair separation are key factors in photocatalytic performance. The UV-vis DRS spectra (Fig. S4a in Supporting information) show that as the reducing agent amount increased, the light absorption edges of BTORX (X = 1, 2, 3) catalysts occurred red-shifted, and the visible light response also increased. It is due to the localized surface plasmon resonance (LSPR) effect of metallic Bi, and the increased absorption confirms more plasmonic metallic Bi presence

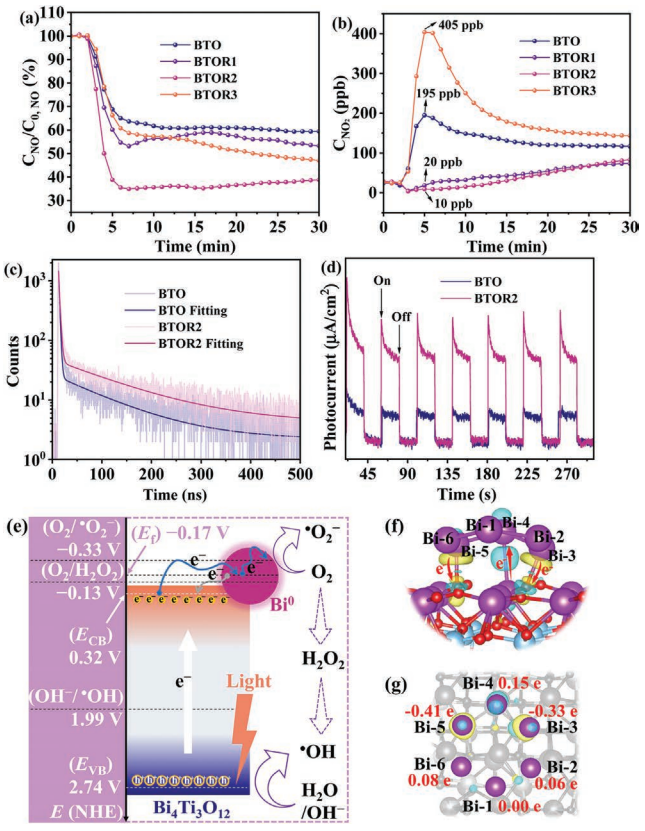



**Fig. 3.** Time-dependent NO concentration for BTO and BTORX (X = 1, 2, 3) (a) and corresponding $NO_2$ increments (b). The ns-level time-resolved fluorescence spectra (c), photocurrent density *vs.* irradiation time (d) for BTO and BTOR2. The photocatalytic active radical species generation process over Bi/$Bi_4Ti_3O_{12}$-OVs (e). The charge density difference (f) and Bader charge (g) between $Bi_4Ti_3O_{12}$ and metallic Bi.

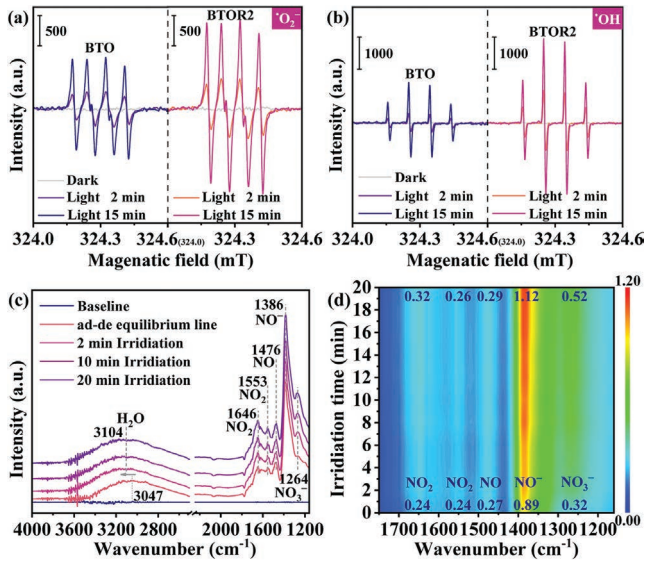



**Fig. 4.** DMPO spin-trapping ESR spectra of BTO and BTOR2 methanol dispersion for DMPO-•$O_2^-$ (a) and aqueous dispersion for DMPO-•OH (b). *In-situ* DRIFTS of photocatalytic NO oxidation over BTOR2 (c) and the heat map of the characteristic peaks change with light exposure time (d).

in modified $Bi_4Ti_3O_{12}$. According to the evaluated band gaps (Fig. S4b) and empirical equations (Eqs. S1 and S2 in Supporting information), the $E_{CB}$ and $E_{VB}$ edges of $Bi_4Ti_3O_{12}$ are calculated to be 0.32 V and 2.74 V, respectively (Supporting information). Figs. S4c and d (Supporting information) show the Bi-O and Bi-Bi bonds in different perspectives (View-1 and View-2 in Supporting information), the electron localized function of Bi/$Bi_4Ti_3O_{12}$-OVs demonstrates strong interaction (marked in red) between $Bi_4Ti_3O_{12}$ and metallic Bi, aiding the transfer of carriers. The charge carrier lifetime is 2.36 ns for BTOR2, longer than the 1.83 ns for BTO (Fig. 3c), indicating better charge mobility. Fig. 3d shows fast photocurrent rise and decay during light-dark cycles, with BTOR2 achieving a higher current than BTO, indicating efficient charge separation and rapid electron migration. The heterojunction between metallic Bi and $Bi_4Ti_3O_{12}$ effectively separates $e^-/h^+$ pairs and promotes carrier transfer.

The process of photocatalytic active radical generation over Bi/$Bi_4Ti_3O_{12}$-OVs is illustrated in Fig. 3e. Electron-hole pairs generated in $Bi_4Ti_3O_{12}$ under light illumination. The $E_{VB}$ of $Bi_4Ti_3O_{12}$ (2.74 V) is more positive than the redox potential of $OH^-/•OH$ (1.99 V), enabling the generation of •OH radicals from adsorbed $H_2O/OH^-$ by holes. The DFT calculation results of charge density difference (Fig. 3f) and Bader charge (Fig. 3g) are analyzed. The quantification and visualization results demonstrate that electrons could transfer between $Bi_4Ti_3O_{12}$ and metallic Bi. The free electrons of metallic Bi (Fermi level is -0.17 V) transfer to the conduction band ($E_{CB}$ = 0.32 V) of $Bi_4Ti_3O_{12}$. Meanwhile, the free electrons of $Bi_4Ti_3O_{12}$ also can jump to metallic Bi by light stimulation in theory. Importantly, the free electrons could be further transited to a more negative energy level than the redox potential of $O_2/•O_2^-$ (-0.33 V) through the light-induced LSPR effect. Thus, the adsorbed $O_2$ could be oxidized to $•O_2^-$ radicals or $H_2O_2$ species ($O_2 + 2e^- + 2H^+ \rightarrow H_2O_2$), and the $H_2O_2$ species could be further transformed into •OH radicals. In summary, •OH and $•O_2^-$ radicals are the primary active species responsible for NO oxidation.

ESR analyses were performed on $Bi_4Ti_3O_{12}$ and BTOR2 to trace active radical species. The results (Figs. 4a and b) show no signal in the dark. Under light, both BTO and BTOR2 exhibit six characteristic peaks of DMPO-$•O_2^-$, with BTOR2 showing stronger intensities (Fig. 4a). Additionally, four characteristic peaks with a 1:2:2:1 intensity ratio were assigned to the DMPO-•OH adduct, with BTOR2 displaying stronger signals than BTO again (Fig. 4b). The results indicate that metallic Bi and oxygen vacancies enhance the production of $•O_2^-$ and •OH radicals.

Based on the described mechanism and experimental findings, the improved photocatalytic efficiency of Bi/$Bi_4Ti_3O_{12}$-OVs composites is attributed to the combined influence of metallic Bi and oxygen vacancies. The photosensitive electrons of $Bi_4Ti_3O_{12}$ will gather on the metallic Bi and migrate upward, thus the LSPR effect of metallic Bi can enhance the surface oxidation performance of the material.

An *in-situ* DRIFTS experiment was conducted at a gas flow rate of 25 mL/min ($C_{NO}$ = 50 ppm) to study the photocatalytic NO oxidation mechanism on Bi/$Bi_4Ti_3O_{12}$-OVs. Fig. 4c shows the time-dependent infrared characteristic peak evolution under light. The baseline represents the background after subtracting the initial material surface peak under the helium atmosphere. After the adsorption and desorption equilibrium was reached on the surface of BTOR2, a series of characteristic peaks appeared (Table S2 in Supporting information). The broad peak at 3047 $cm^{-1}$ is assigned to adsorbed $H_2O$ (O-H stretching vibration) [37], and peaks at 1476 $cm^{-1}$, 1646 $cm^{-1}$, and 1553 $cm^{-1}$ correspond to NO and $NO_2$ molecules [38,39]. The NO molecule is activated into $NO^-$ (detected at 1386 $m^{-1}$) after electron transfer [40,41]. Under light irradiation, the $H_2O$ peak shifts to 3104 $cm^{-1}$, indicating enhanced adsorption strength and contributing to •OH radical generation. The $NO_3^-$ peak at 1264 $cm^{-1}$ [42] confirms the deep photocatalytic oxidation of NO to $NO_3^-$. Fig. 4d shows the heat map of peak changes with light exposure time. After illumination, NO and $NO_2$ accumulate slightly,

while $NO^-$ intensity increases from 0.89 to 1.12, indicating the activation of NO to $NO^-$ and subsequent oxidation to $NO_3^-$. The intensity of $NO_3^-$ increased from 0.32 to 0.52, confirming successful purification of $NO/NO_2$.

In summary, this work presents a unique plasmonic metallic Bi-modified defective $Bi_4Ti_3O_{12}$ nanosheets catalyst. The LSPR effect of metallic Bi and the abundant oxygen defects in the as-synthesized $Bi/Bi_4Ti_3O_{12}$-OVs materials lead to enhanced visible light absorption and improved photogenerated carrier migration compared to the original $Bi_4Ti_3O_{12}$. DFT calculations of the electron local function reveal a strong interaction between the surface metallic Bi and the $Bi_4Ti_3O_{12}$ substrate, facilitating the transfer of photogenerated carriers. Moreover, the quantitative Bader charge and visualize charge density difference analysis results further demonstrate that free electrons can migrate from $Bi_4Ti_3O_{12}$ to metallic Bi, with subsequent jump to higher energy level beyond the $E_{redox}$ of $O_2/^{\bullet}O_2^-$, promoting conversion of $O_2$ to $^{\bullet}O_2^-$ radicals. The *in-situ* DRIFTS analysis demonstrates that the $Bi/Bi_4Ti_3O_{12}$-OVs can respond to light rapidly for the adsorption strength enhancement of $H_2O$ molecules, which benefits the generation of $^{\bullet}O_2^-$ radicals. The key intermediate species, $NO^-$, was further traced, and its highly reducing state leads it to be oxidized to $NO_3^-$ more readily than NO. The results show that the optimized metallic Bi-modified defective $Bi_4Ti_3O_{12}$ nanosheets catalysts exhibit excellent photocatalytic performance (62.3 %) while minimizing toxic $NO_2$ formation for stable deep NO oxidation. This study offers significant insights that can enhance research on effective photocatalysts for controlling air pollution.

## Declaration of competing interest

The authors declare that they have no known competing financial interests or personal relationships that could have appeared to influence the work reported in this paper.

## CRediT authorship contribution statement

**Wenjie He:** Writing – original draft, Methodology, Funding acquisition, Formal analysis, Data curation, Conceptualization. **Lin Jing:** Writing – review & editing, Investigation, Data curation. **Wendong Zhang:** Methodology. **Xing'an Dong:** Funding acquisition, Formal analysis, Data curation. **Yan Zou:** Data curation. **Xin Liu:** Formal analysis. **Xin Lv:** Formal analysis. **Peng Chen:** Methodology, Formal analysis. **Jiazhen Liao:** Methodology, Funding acquisition. **Xiao Zhang:** Investigation. **Rong Xiao:** Investigation. **Yuechang Wei:** Writing – review & editing, Methodology, Conceptualization.

## Acknowledgments

This research is financially supported by the Natural Science Foundation of Chongqing (Nos. CSTB2024NSCQ-MSX1278, CSTB2023NSCQ-MSX0006), Technology Innovation Project of Shapingba District, Chongqing (No. 2024004), Science and Technology Research Program of Chongqing Municipal Education Commission (Nos. KJZD-K202403102, KJQN202103110, KJQN202400512, KJQN202403107), National Natural Science Foundation of China (No. 22406014); China Postdoctoral Science Foundation (No. 2023MD744137).

## Supplementary materials

Supplementary material associated with this article can be found, in the online version, at doi:10.1016/j.cclet.2025.111357.

## References

[1] S. Ahmad, L. Liu, S. Zhang, J. Tang, J. Hazard. Mater. 446 (2023) 130727.
[2] D. Yuan, M. Sun, S. Tang, et al., Chin. Chem. Lett. 31 (2020) 547–550.
[3] K. Su, T. Gao, C. Tung, L. Wu, Angew. Chem. Int. Ed. 63 (2024) e202407464.
[4] Y. Wu, Y. Xu, Y. Zhang, et al., Chin. Chem. Lett. 33 (2022) 2741–2746.
[5] G. Gan, Z. Yang, Y. Li, G. Zhang, Appl. Catal. B: Environ. 357 (2024) 124308.
[6] K. Wang, S. Zeng, G. Li, et al., Appl. Catal. B: Environ. 343 (2024) 123565.
[7] J. Li, Y. Li, X. Wang, Z. Yang, G. Zhang, Chin. J. Catal. 51 (2023) 145–156.
[8] L. Sun, D. Wang, Y. Li, et al., Chin. Chem. Lett. 34 (2023) 107490.
[9] C. Xiao, G. Dong, T. Liu, L. Wang, C. Zhu, Sep. Purif. Technol. 347 (2024) 127673.
[10] W. Qin, Y. Xiao, C. Zhang, H. Gong, Q. Zhang, Q. Zeng, Chem. Eng. J. 490 (2024) 151511.
[11] Y. Wang, J. Wang, Q. Zhu, et al., J. Environ. Chem. Eng. 12 (2025) 115046.
[12] L. Huang, X. Huang, J. Yan, et al., J. Hazard. Mater. 442 (2023) 130024.
[13] J. Wang, J. Wang, S. Zuo, J. Pei, W. Liu, et al., Chin. Chem. Lett. 34 (2023) 108157.
[14] H. Kaur, S. Singh, B. Pal, Appl. Surf. Sci. 609 (2023) 155455.
[15] J. Geng, L. Zhao, M. Wang, G. Dong, W. Ho, Environ. Sci. Nano 9 (2022) 742–750.
[16] J. Liao, K. Li, H. Ma, et al., Chin. Chem. Lett. 31 (2020) 2737–2741.
[17] C. Yuan, W. Cui, Y. Sun, et al., Chin. Chem. Lett. 31 (2020) 751–754.
[18] J. Murillo-Sierra, R. Romero, V. Melin, et al., ChemSusChem 18 (2025) e202401489.
[19] Q. Zhu, Y. Wang, J. Wang, J. Luo, J. Xu, et al., Appl. Catal. B: Environ. 346 (2024) 123734.
[20] Z. Liu, G. Li, M. Zhang, et al., J. Colloid. Interface Sci. 675 (2024) 721–730.
[21] Z. Liu, Y. An, W. Zhang, L. Zhu, G. Zhu, J. Alloys Compd. 942 (2023) 169018.
[22] Q. Zhu, R. Hailili, Y. Xin, et al., Appl. Catal. B: Environ. 319 (2022) 121888.
[23] W. He, J. Xiong, Z. Tang, et al., Appl. Catal. B: Environ. 344 (2024) 123651.
[24] G. Gan, Y. Li, G. Zhang, Sep. Purif. Technol. 355 (2025) 129587.
[25] J. Yang, L. Li, C. Xiao, Y. Xie, Angew. Chem. Int. Ed. 62 (2023) e202311911.
[26] Z. Yang, H. Wang, X. Hao, L. Zhang, Y. Li, et al., J. Mater. Sci. Technol. 216 (2025) 27–37.
[27] K. Sharma, A. Kumar, T. Ahamad, et al., J. Mater. Sci. Technol. 152 (2023) 50–64.
[28] F. Sun, Q. Xu, H. Liu, et al., J. Catal. 440 (2024) 115813.
[29] Y. Kong, D. Li, C. Zhang, et al., Chem. Eng. J. 479 (2024) 147676.
[30] X. Kang, G. Dong, T. Dong, ACS Appl. Energy Mater. 6 (2023) 1025–1036.
[31] F. Li, G. Liu, F. Liu, J. Wu, S. Yang, J. Hazard. Mater. 452 (2023) 131237.
[32] Y. Sun, H. Ji, Y. Sun, et al., Angew. Chem. 136 (2024) e202316973.
[33] Q. Zhu, A.A. Dar, Y. Zhou, ACS EST Eng. 2 (2022) 1365–1375.
[34] D. Zu, Y. Ying, Q. Wei, et al., Angew. Chem. Int. Ed. 63 (2024) e202405756.
[35] X. Li, K. Li, D. Ding, et al., Sep. Purif. Technol. 309 (2023) 123054.
[36] R. Du, K. Xiao, S. He, Y. Wang, C. Kang, J. Alloys. Compd. 955 (2023) 170168.
[37] N. Yang, R.M. Huchmala, A.B. McCoy, M.A. Johnson, J. Phys. Chem. Lett. 13 (2022) 8116–8121.
[38] K.I. Hadjiivanov, Catal. Rev. 42 (2000) 71–144.
[39] S.J. Huang, A.B. Walters, M.A. Vannice, J. Catal. 192 (2000) 29–47.
[40] Y. Xin, Q. Zhu, T. Gao, et al., Appl. Catal. B: Environ. 324 (2023) 122238.
[41] C. Feng, P. Wang, X. Liu, et al., Environ. Sci. Technol. 55 (2021) 11255–11264.
[42] W. Zhang, X. Liu, X. Dong, F. Dong, Y. Zhang, Chin. J. Catal. 38 (2017) 2030–2038.